IJMMM International Journal of Minerals, Metallurgy and Materials 矿物冶金与材料学报（英文版）

Effect of transport agent boron triiodide on the synthesis and crystal quality of boron arsenide

Zhenxing Liu, Fangjie Deng, Yuan Zhou, Yanjie Liang, Cong Peng, Bing Peng, Feiping Zhao, Zhihui Yang, and Liyuan Chai

Cite this article as:
Zhenxing Liu, Fangjie Deng, Yuan Zhou, Yanjie Liang, Cong Peng, Bing Peng, Feiping Zhao, Zhihui Yang, and Liyuan Chai, Effect of transport agent boron triiodide on the synthesis and crystal quality of boron arsenide, *Int. J. Miner. Metall. Mater.*, 29(2022), No. 4, pp. 662-670. https://doi.org/10.1007/s12613-022-2438-z

---

International Journal of Minerals, Metallurgy and Materials
Volume 29, Number 4, April 2022, Page 662
https://doi.org/10.1007/s12613-022-2438-z

Effect of transport agent boron triiodide on the synthesis and crystal quality of boron arsenide

Zhenxing Liu[1)], *Fangjie Deng*[1)], *Yuan Zhou*[1)], *Yanjie Liang*[1,2),✉], *Cong Peng*[1,2)], *Bing Peng*[1,2)], *Feiping Zhao*[1,2)], *Zhihui Yang*[1,2)], *and Liyuan Chai*[1,2),✉]

1) School of Metallurgy and Environment, Central South University, Changsha 410083, China
2) Chinese National Engineering Research Center for Control & Treatment of Heavy Metal Pollution, Changsha 410083, China
(Received: 10 January 2022; revised: 12 February 2022; accepted: 15 February 2022)

Abstract: Cubic boron arsenide (BAs) has attracted great attention due to its high thermal conductivity, however, its controllable, stable, and ideal preparation remains challenging. Herein, we investigated the effect of iodine-containing transport agents I_2 and boron triiodide (BI_3) on BAs synthesized and grown through chemical vapor transport. Results show that similar to the commonly used I_2, BI_3 accelerates the synthesis and improves the mass fraction of BAs from ~12% to over 90% at 820°C and 1.5 MPa, a value beyond the promoting effect of only increasing temperature and pressure. Both agents enhance the quality of BAs crystals by reducing the full width at half maximum by up to 10%–20%. I_2 agglomerates the grown crystals with twin defects (~50 nm wide), and BI_3 improves the crystal anisotropy and element uniformity of BAs crystals with narrow twins (~15 nm wide) and increases the stoichiometry ratio (~0.990) to almost 1. Owing to the boron interstitials from the excessive boron supply, the spacing of layers in {111} increases to 0.286 nm in the presence of I_2. Owing to its coordinated effect, BI_3 only slightly influences the layer spacing at 0.275 nm, which is close to the theoretical value of 0.276 nm. In the chemical vapor transport, the anisotropic crystals with flat surfaces exhibit single-crystal characteristics under the action of BI_3. Different from that of I_2, the coordinated effect of BI_3 can promote the efficient preparation of high-quality BAs crystal seeds and facilitate the advanced application of BAs.

Keywords: boron arsenide; transport agent; boron–arsenic reaction; iodine; boron triiodide

1. Introduction

Cubic boron arsenide (BAs) crystals with high experimental thermal conductivity of ~1300 W/m·K [1–2] can improve the performance of microelectronics [3]; however, its stable and controllable preparation is challenging. High-quality BAs crystals with a theoretically appropriate stoichiometric ratio and few defects have excellent applications [4–7] and are essential in the mass production of cubic BAs crystals when used as seeds. Nevertheless, the slow solid-state (gas–solid) reaction rate [8] for BAs synthesis and the tendency to form polycrystals [9–10] complicate the preparation of suitable crystal seeds.

The efficient synthesis of high-quality crystals constrains the production and application of BAs. Whiteley *et al.* [11] tried to prepare boron-rich compounds using a nickel flux method but only obtained boron subarsenide ($B_{12}As_2$). Thermodynamic theory indicates that $B_{12}As_2$ is stable at temperatures greater than 920°C [12]. At below 920°C, only substable BAs compounds can be obtained using widely applied high-temperature synthesis methods with gaseous arsenic and solid boron [8,13]. A convenient technique to improve the quality and yield of single crystal in deposition is to use a crystal seed. Chemical vapor transport (CVT) is a promising technology to produce high-quality BAs crystals and seeds. However, this route requires a long period of up to weeks or even months and involves a multistep hand-picking process [2,13–18]. In addition, the reported synthesis methods share the characteristics of slow synthesis rate, polycrystalline particles, and defective structures, which are thought to be related to the fluctuation of components during mass transfer [19–21]. The use of transport agents has greatly improved the efficiency of the reaction and growth. The commonly used transport agent I_2 allows the transport efficiency of the boron source to reach ~90% [16]. Other effective transport agents include AsI_3 [20], TeI_4 [21], and NH_4I [19]. Elemental iodine halogenates the boron source to produce gaseous B–I compounds [19–21]. The shift in the boron-binding form converts the mass transfer process from solid-state diffusion to gaseous convection. However, defective crystal structures, such as twins [22], vacancies [5,13], interstitial atoms, and anti-sites [7,23], still occur and cause the stoichiometric ratio to deviate from the theoretical value of 1 [9]. Solid-source boron, even when effused at 1700–1800°C, eventually segregates in other gaseous deposition systems, such as molecular beam epitaxy [24–25]. This segregation might be re-

✉ Corresponding authors: Yanjie Liang E-mail: LiangyanjieCSU@163.com; Liyuan Chai E-mail: lychai@csu.edu.cn

lated to the production of boron-rich subarsenide compounds [25]. To date, the suppression of structural defects associated with mass transfer remains poorly studied. Especially for BAs, iodine-containing transport agents are effective for the mass transfer of the boron source. However, defects occur occasionally, and this problem might be related to the type of transport agent that affects the incorporation of boron and arsenic. Hence, the type of transport agent is crucial for the efficient synthesis of high-quality compounds and crystal seeds of BAs.

In this work, we apply a new transport agent, boron triiodide (BI_3), and investigate its effect on the solid-state reaction between boron and arsenic and the crystal growth behavior. We provide an alternative route for the efficient synthesis of high-quality BAs crystals in the future.

2. Experimental

2.1. Synthesis and growth of BAs crystals

BAs crystals were synthesized as follows. High-purity metallic natural boron powders (B, 99.999wt%, Aladdin) and pure metallic arsenic lumps (As, 99.9999wt%, DONGFANG Electric) with iodine particles (I_2, 99.995wt%, Aladdin) or boron triiodide (BI_3, >98wt%, Alfa Aesar) were placed at one end of a fused quartz tube inside an Ar-flowed glovebox (H_2O < 0.000001%, O_2 < 0.000001%) with an atomic ratio of As : B = 2.2. The atomic percentages of iodine were set at 0.0at%, 1.3at% and 2.5at%. The ratio of As : B was selected based on a previous study [9]. The quartz tube has a 20 mm length, 2 mm thickness, and 16 mm inner diameter. Reaction pressure P was estimated using the formula $P = nRT/V$, MPa, where n is the mole of gases (As_4, AsI_3, I_2, and BI_3), mol; T is the reaction temperature, K; V is the tube volume, mm^3; and R is the universal gas constant, 8.314 $J{\cdot}mol^{-1}{\cdot}K^{-1}$. Different reaction pressures P = 0.1, 0.3, 0.7, and 1.5 MPa were investigated.

BAs samples were synthesized through solid-state reactions. The quartz tube was evacuated and then flame-sealed in a high vacuum (~0.01 Pa). The containers were placed in a horizontal two-zone tube furnace for B–As reaction and CVT growth. Finally, the mixed raw materials in the B–As reaction batches were placed in a one-temperature zone with two zones of the same temperature for 3 d, and the temperatures were configured at 780, 820, 860, and 915°C.

The crystals were grown using the CVT method. The tube with raw materials was placed in the high-temperature zone at 890°C, and the SiO_2 (0001) substrate was positioned in the low-temperature zone at 800°C for 15 d to grow BAs crystals. The temperature accuracy varied by ±1°C. The furnace was heated to 620°C first at 1°C/min and then at 0.33°C/min to the target holding temperature and cooled to room temperature below 150°C. The excessive arsenic lumps were manually removed, and the products were cleaned with dilute nitric acid, deionized water, and ethyl alcohol for further analysis.

We summarize the chemical reactions of boron and arsenic as follows:

Without an agent, $B(s) + 0.25As_4(g) \xrightarrow{\Delta} BAs(s)$;

With I_2 [14,20–21,26], $1.5I_2(g) + BAs(s) \overset{\Delta}{\leftrightarrow} 0.25As_4(g) + BI_3(g)$;

With BI_3, $BI_3(g) + BAs(s) \overset{\Delta}{\leftrightarrow} 0.25As_4(g) + BI_3{\cdot}B(g)$.

2.2. Characterization

We performed X-ray diffraction (XRD) on a Rigaku TTR III X-ray diffractometer with a Cu K_α radiation source. The 2θ angle scanning range was 15°–90°, and the scanning speed was 6°/min. The diffraction patterns were analyzed and refined with the software package MDI Jade 6.5 to obtain the full width at half maximum (FWHM) of the BAs plane (111). Peak area data were correlated to the crystal quality and used for the semiquantitative calculation of BAs fraction using the RIR method in the supporting information.

We performed the vibration spectrum analysis of BAs crystals on a confocal Raman spectrometer (inVia, Renishaw, UK) with a laser wavelength of 532 nm. The input power was set to ~25 mW to avoid overheating the sample, and a 50× objective lens (Numerical Aperture = 0.5) collected the backscattered signals. The diameter of the light spot on the sample surface was 2–5 μm. For each sample, at least five points were collected and graphed in a box plot to analyze the dispersion range. The data were processed using the Origin software package to obtain the FWHM of fingerprint peak P1 with the PsdVoigt1 function for peak fitting.

We observed crystalline structures by scanning electron microscopy (SEM) and transmission electron microscopy (TEM). SEM imaging was implemented on a field emission scanning electron microscope (Nova NanoSEM230, FEI, USA) with energy dispersive X-ray spectroscopy (EDS) using an accelerating voltage of 18 kV for backscattered electron imaging (BSE). A two-beam scanning electron microscope equipped with a focused ion beam machine (Helios Nanolab, G3 UC FEI, USA) was used to prepare TEM samples. The sheet sample was cut from a bulk BAs crystal and milled with a Ga ion beam until the sample was thin enough (<100 nm) to be traversed by the electron beam for TEM testing. The sample was cleaned by an ion beam at low voltage and then observed at 300 kV with an aberration-corrected TEM (Titan G2 60-300, FEI, USA) equipped with EDS. TEM images and related analyses were processed with Gatan software.

We employed an optical microscope (DSX500, Olympus, Japan) to observe the crystal morphology of BAs on the SiO_2 substrate. Dynamic focusing and imaging at bright–dark mixed differential interference contrast (DIC) mode were performed along the height dimension to collect a three-dimensional image.

3. Results and discussion

3.1. Characteristics of BAs crystals synthesized through solid-state reaction

3.1.1. Effect of reaction pressure and temperature

The chemical reaction between boron and arsenic only occurs at the gas–solid interface and is influenced by thermal

dynamic factors, namely, temperature and pressure. Metallic arsenic sublimates to gas As_4, but metallic boron with low saturated vapor pressure and high melting point is hardly volatile [27]. XRD patterns in Fig. 1 show the products after the solid-state reaction. The products match well with the diffraction peaks of boron (PDF 80-0324) and BAs (PDF 03-004-5090). The peaks of BAs are symmetrical, and the main peak's intensity increases with the reaction pressure, as shown in Fig. 1(a). The BAs crystals crystallize well with increasing pressure. Based on the ratio of products, we obtained the mass fraction of BAs after fitting and refining with Jade software. The fraction of BAs in Fig. 1(b) increases linearly from 3.8% ± 0.4% (P = 0.1 MPa) to 12.1% ± 1.1% (P = 1.5 MPa). Although the solid-state reaction between boron and arsenic is slow, it is positively related to the reaction pressure. When the pressure is retained at 1.5 MPa (Fig. 1(c)), the intensity ratio of the main diffraction peak between boron and BAs gradually increases with temperature. When the reaction temperature reaches 915°C, the peak intensity of the boron powders almost disappears, indicating the maximum conversion ratio of boron. As shown in Fig. 1(d), the mass fraction of BAs varies from 12.3% ± 0.5% at 780-820°C to 87.5% ± 5.0% at 920°C. These results suggest that although high reaction pressure and temperature can accelerate the solid-state reaction between boron and arsenic, the effect has further room for improvement.

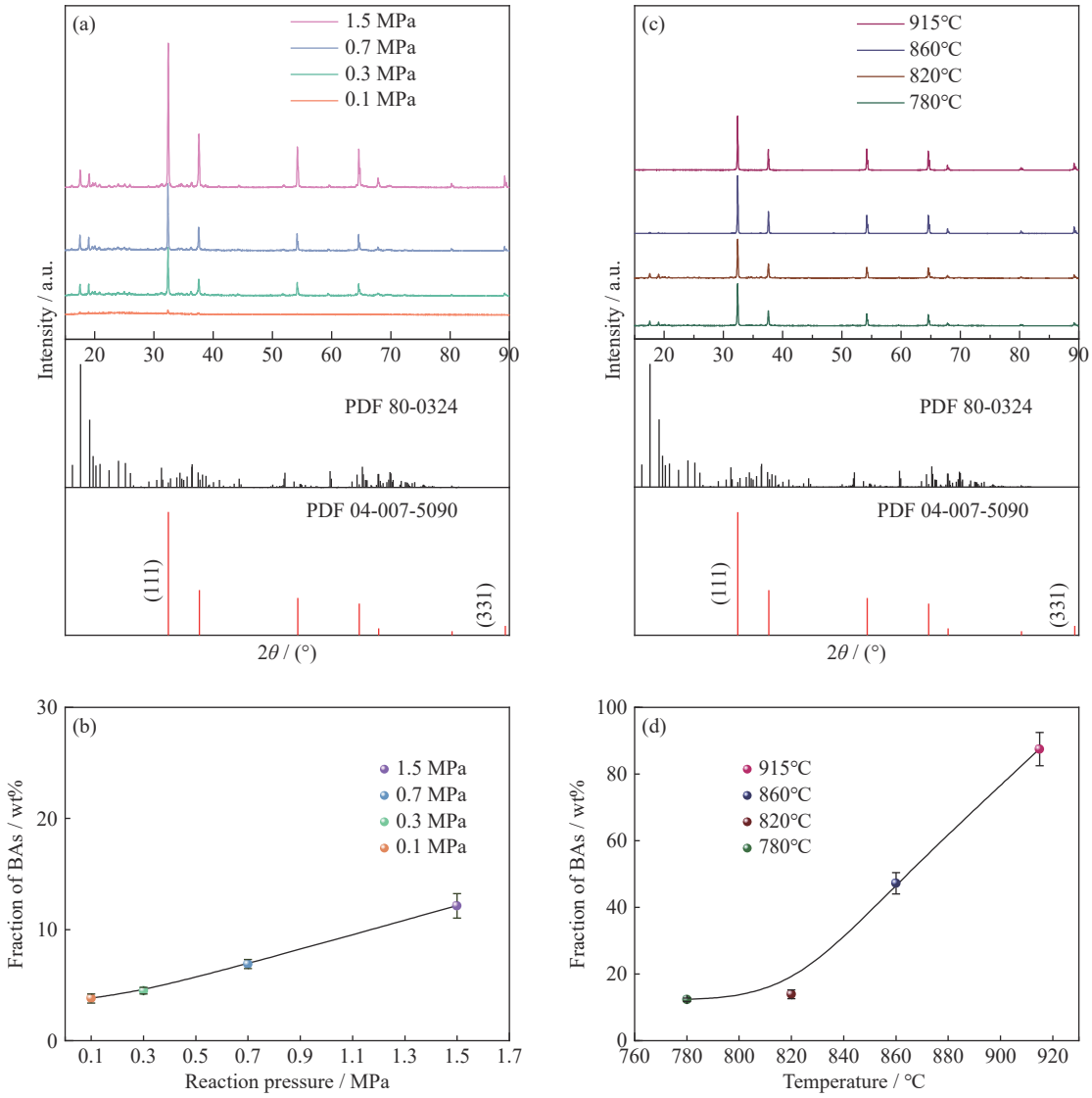

Fig. 1. XRD patterns of BAs in the solid-state reaction: (a) under different pressures at 820°C; (c) at different reaction temperatures under 1.5 MPa. (b, d) Mass fraction of BAs in (a) and (c) calculated by RIR method. PDF 80-0324 and PDF 04-007-5090 belong to boron powder and BAs, respectively.

3.1.2. Effect of the transport agents

To further improve the synthesis efficiency, we examined the effect of the new agent. Iodine-containing transport agents can significantly enhance the solid-state reaction between boron and arsenic. As shown in Fig. 2(a), the characteristic peaks' intensity of BAs increases with the rising reaction pressure and iodine atoms concentration. It is enhanced slightly by increasing the pressure from 0.3 to 0.7 MPa at the same iodine concentration. However, the synthesis efficiency of BAs is closely related to the element iodine.

The peaks in batches reacting under 0.7 MPa appear significant. The enlarged view ranging from 15° to 20° in Fig. 2(b) shows that the characteristic peaks of boron powders gradually decrease, indicating that the transformation efficiency of boron improves sharply. With reaction pressures up to 1.5 MPa, the peaks of the boron powders almost disappear. Especially in batches with agent BI_3 at a dose of 2.5at% I, the pressure can be reduced to 0.7 MPa to eliminate the peaks of boron powders. The calculated fraction of BAs in Table S1 is over 90% under 1.5 MPa in the presence of I_2 or BI_3. The agents can increase the production by 6–10 times compared with batches with no addition. Halogenation can effectively accelerate the mass transport of boron sources [28–29]. We confirm that intermediate BI_3 can also realize the mass transport of boron powders. As a result of gasification at high temperature, B–I compounds convert the gas–solid interface reaction into a gas–gas reaction between metallic boron and arsenic. The distinct acceleration effect between I_2 and BI_3 is based on their different molecular affinities to metallic boron in the reaction. In theory, BI_3 more easily sticks to the boron surface and react with boron powder than I_2 because the contained boron atom forms a transition state BI_3·B to speed up boron transport. Similar to the commonly used I_2, BI_3 accelerates the reaction rate even under low pressure at 820°C.

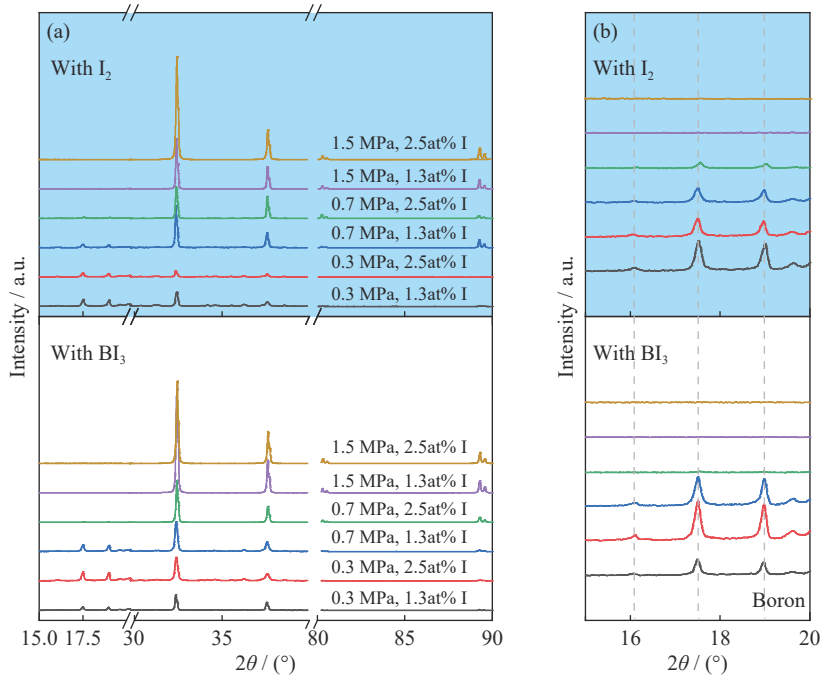

Fig. 2. (a) XRD patterns of products under the action of transport agents I_2 and BI_3 at various reaction pressures and 820°C for 3 d; (b) partially enlarged view of XRD patterns (gray dashed lines point to the diffraction peaks of boron in the range of 15°–20°).

3.2. Evolution of crystalline morphology under the action of transport agents

In addition to accelerating the reaction, the ability of transport agents to change the crystal features should be considered carefully, especially for BI_3. The results in Fig. 3 (at 820°C under 1.5 MPa) show that transport agents change the growth and agglomeration features of BAs crystals. The reaction without agents disperses few small BAs crystals with a size of approximately 5 μm on the coral-shaped boron powders. These crystals gather together similar to small grapes (Fig. 3(a)). After BI_3 or I_2 is added, the BAs crystals become the dominant phase (Fig. 3(b) and (c)). A small number of unreacted B powders can be found around the BAs crystals in both experimental batches and are not detected by XRD due to their low content. Crystals gather around similar to apples under the action of I_2 and agglomerates into spherical polycrystals with a size over 50 μm. Many boundaries (indicated by yellow arrows) appear on the crystal surface. When BI_3 is added to the reaction, the growth of BAs individual polyhedral crystals can be considered because of the evident facets between individual crystals (Fig. 3(c)). An individual crystal after physical dispersion is shown in Fig. 3 and is identified as a polyhedron consisting of facets without distinct boundaries on the surfaces. In addition, the different transport effects of agents on element boron are reflected. Table 1 shows that the average atomic ratio of boron and arsenic in BAs crystals is 55.54:41.83 (the stoichiometry ratio is 1.328) in Fig. 3(b) and 49.28:50.16 (the stoichiometry ratio is 0.982) in Fig. 3(c). Impurities such as Si and I can also be detected. The large crystal size implies the intense transport effect of I_2 and BI_3 on boron. Nevertheless, BI_3 can coordinate the uniform incorporation behavior of arsenic and boron in a polyhedron shape.

3.3. Role of transport agent BI_3 on boron–arsenic crystal growth

3.3.1. Improving the crystalline property

Given the enhancement of the reaction efficiency and the changes in the morphological characteristics, the synthesis process was optimized to improve the crystal quality. The

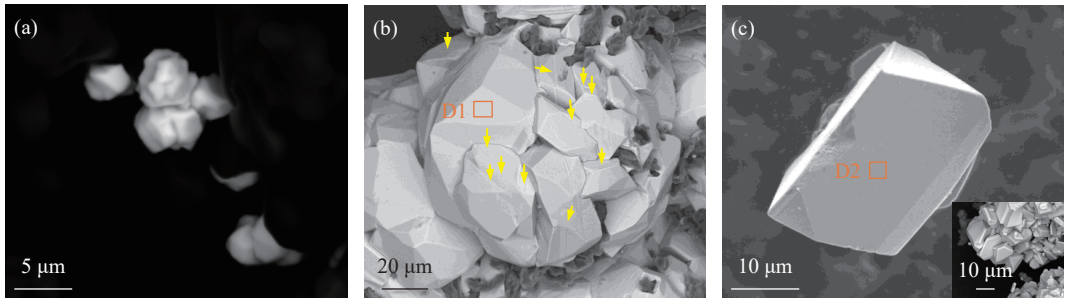

Fig. 3. SEM graphs (BSE) of BAs crystals synthesized at 820°C and 1.5 MPa: (a) with no addition; with (b) I_2 and (c) BI_3 at a dose of 2.5at% I. The inset in (c) shows the undispersed state. Yellow arrows indicate boundaries on the crystal surface.

Table 1. Composition of elements in district D1 and D2 in Fig. 3(b) and (c) from the EDS spectra

Element	D1		D2	
	Content / at%	y in B_yAs	Content / at%	y in B_yAs
B	55.54	1.328	49.28	0.982
Si	0.13		0.46	
I	2.50		0.10	
As	41.83		50.16	

Raman spectra in Fig. 4(a) show the typical vibration curves of BAs. We located the fingerprint peak P1 of BAs crystal at the wavenumber 699–702 cm^{-1}, which refers to the theoretical peak P1 for ^{nat}BAs (704 cm^{-1}, using the natural boron) [30]. We analyzed the FWHMs for the main peak (plane (111)) in the XRD patterns of the samples (obtained at 820°C and under 1.5 MPa) and for the peak P1 in Raman spectra to investigate the quality of BA crystals [14,26,31–32]. After the iodine-containing transport agent is added, the average FWHM of plane (111) decreases from ~0.14° to ~0.11° in Fig. 4(a), indicating the improved crystallinity of BAs. This finding is consistent with Fig. 2. However, the histograms (blue color) in Fig. 4(b) reflect minimal difference between the influences of I_2 and BI_3. The addition of agents (BI_3 or I_2) enhances the order of the synthesized BAs crystals. The average FWHM of peak P1 in Raman spectra shares the same trend as that of plane (111) in XRD patterns. Given that the microzone order (from Raman spectra) is consistent with macrocrystallinity (from XRD patterns), the agents act uniformly and the FWHM values vary in a narrow range. The decrease in average FWHM is up to 10%–20%, implying a non-negligible optimization of crystallization for BI_3. Similar to I_2, BI_3 also improves the crystallinity and order structure of BA crystals. We found a Raman shift of ~3 cm^{-1} under the action of I_2 and BI_3 compared with that for the samples with no addition. This shift is associated with disorders originating from defects [33–34], and its magnitude can be suppressed by I_2 and BI_3.

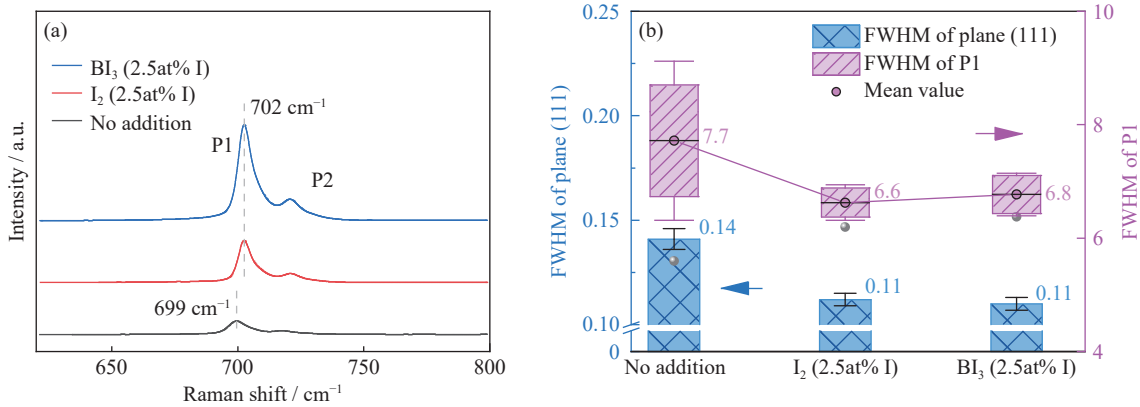

Fig. 4. (a) Raman spectra of boron–arsenic crystals and (b) quality evaluation of BAs crystals synthesized at 820°C with various transport agents. FWHMs of plane (111) in XRD patterns (blue histograms) and fingerprint peak P1 in Raman spectra (pink boxes) were meaasured for crystal quality evaluation; the Raman spectra of BAs crystals are fitted with fingerprint peak P1 using the function PsdVoigt1 in a chi-square tolerance of 10^{-6}.

3.3.2. Suppressing structural defects and maintaining the stoichiometry ratio

Raman spectra reflect the suppression of structural disorders in Fig. 4(a), and the details of the defective structure should be discussed to provide insights into the variation. The inner structure of the obtained BAs crystal is affected by the agents, especially BI_3, because of the crystal's distinctive polyhedron shape. The individual crystal particles shown in Fig. 3(c) may infer a few defects. TEM was employed to gain insights into the microstructures and components of the BAs crystals and observe their internal structure. The scanning transmission electron microscopy (STEM) image reveals many parallel bright and dark lines in the range of ~120 nm in the crystal with no addition. In addition to twin crystal characteristics, twin-like stacking faults are indicted by streaking (white arrows) in the selected area electron diffrac-

tion (SAED) patterns (inset in Fig. 5(a)). Although both agents can eliminate the bright and dark lines (Fig. 5(b) and (c)), sheet-shaped twin crystals remain with widths of ~50 nm in the presence of I_2 and ~15 nm in the presence of BI_3. Under the action of I_2 and BI_3, the formed BAs crystals exhibit distinct internal structures. A line profile of elemental boron and arsenic was implemented across the defective area (yellow line) to explore the variation of mass transfer. The stoichiometry ratio of BAs (denoted as B_yAs) along the line is displayed in Fig. 5(d)–(e). The calculated y value in B_yAs is 0.717 ± 0.015 in BAs crystal with no addition, 1.791 ± 0.029 in BAs with I_2, and 0.990 ± 0.021 in BAs with BI_3. The stoichiometry ratio of BAs regulated by BI_3 is the closest to the theoretical value of 1. In addition, the lattice parameters near the twin boundary have changed. Owing to the light weight of boron, the high-angle annular dark field images (HAADF) in Fig. 5(g)–(i) reflect only arsenic sites in the atomic structure with coherent twin boundary (CTB). The spacing of layers in {111} increases from 0.280 nm in the absence of agents to 0.286 nm in the presence of I_2. Meanwhile, BI_3 only slightly affects the layer spacing at 0.275 nm (the theoretical value of 0.276 nm). For the samples without addition, the deficient boron supply can lead to local arsenic agglutination, and anti-site defects can easily occur to enlarge the spacing [7,23]. In the presence of agents, iodination promotes the mass transfer of boron (section 3.1.2). Considering the small atomic radius of boron, we infer the formation of boron interstitials at high temperatures. The excessive boron or arsenic supply accompanies the increase in lattice parameters, but almost no stacking faults remain when boron is excessive. We

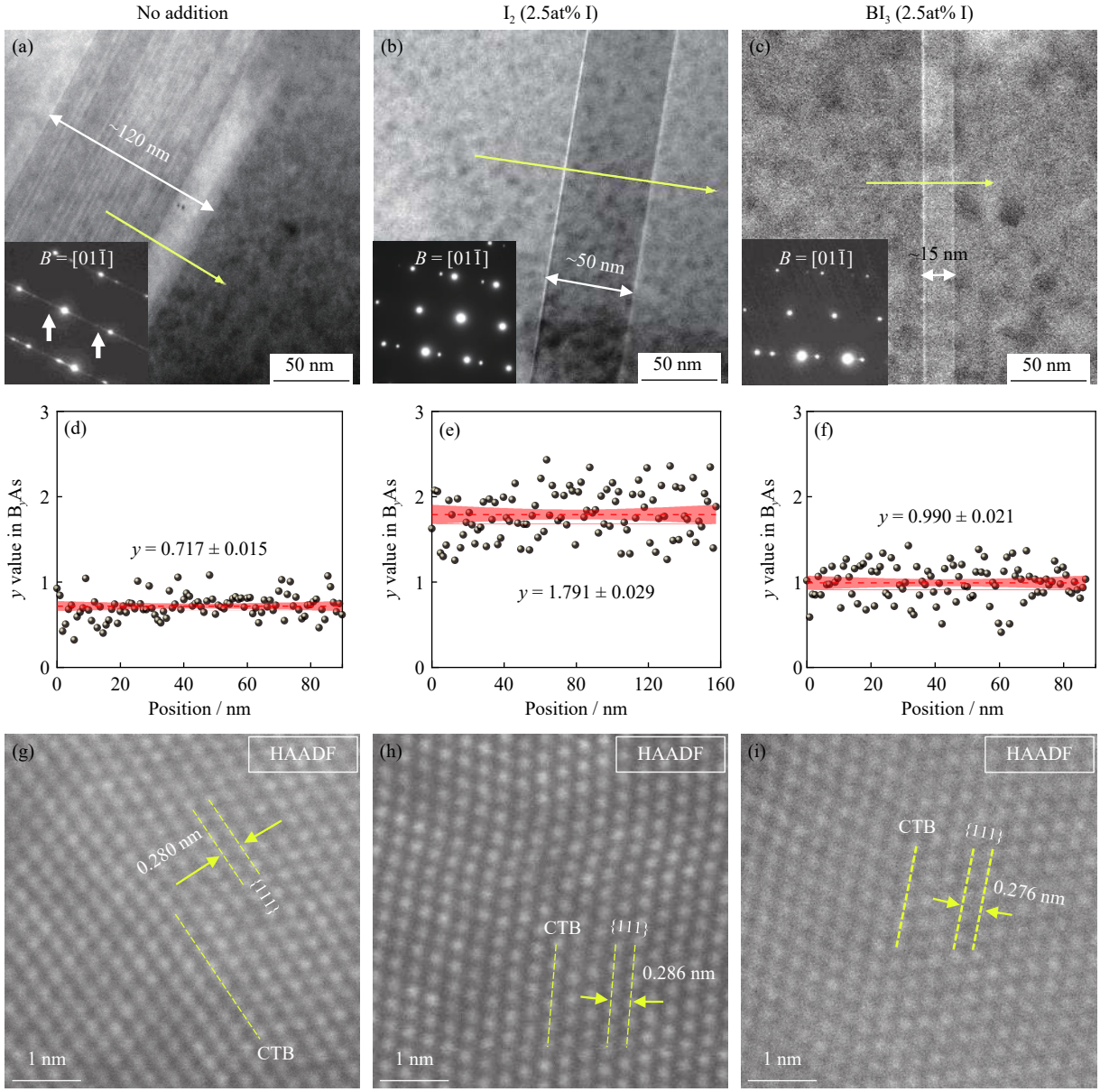

Fig. 5. STEM images of BAs crystals synthesized at 820°C and 1.5 MPa with no agent (no addition) (a), with I_2 (b) and BI_3 (c) at a dose of 2.5at% I; (d, e, f) corresponding y values in B_yAs along the yellow line; (g, h, i) corresponding HAADF images and the layer spacing of {111} near the coherent twin boundary (CTB). The insets in (a), (b), and (c) are SAED patterns, and white arrows pointed to the streaking indicate staking faults along the twin plane {111}. Observation direction is $B = [01\bar{1}]$.

speculate that the excessive boron supply may eliminate the stacking faults but contribute to twin formation. However, BI_3 suppresses the formation of boron interstitials in lattice and coordinates the incorporation of boron and arsenic, besides providing the adequate boron supply. The matching supply of boron and arsenic facilitates the ordered growth of crystal and reduces the defects to maintain anisotropic growth. The suppression is probably related to the interaction between faults and boron atoms, which will be discussed in detail in upcoming work. We conclude that I_2 transfers excessive boron to grow the twins and causes significant deviations in the stoichiometric ratio. Meanwhile, BI_3 can regulate the mass transfer to coordinate the ratios. Both agents can suppress the lack of boron atoms to be incorporated with arsenic, a phenomenon that commonly occurs in cases without agent action. Therefore, few and thin twin grains are formed under the action of BI_3, and uniform chemical components are achieved in the BAs crystal. The increased uniformity might benefit single-crystal growth.

We continued growing the BAs crystal on a substrate (SiO_2 (0001)) in the CVT for 15 d to verify the effect of transport agents, especially BI_3, on single-crystal growth. DIC optical microscope (Fig. 6) was used to determine the single-crystal growth trend of BAs. Few planar defects in the crystal indicate a uniform contrast of the image. The results in Fig. 6 show that the effect of I_2 (Fig. 6(a)–(d)) differs greatly from that of BI_3 (Fig. 6(e)–(h)). Owing to the aggregated effect of I_2 (in Fig. 3(b)), the number of particles in Fig. 6(a) is less than that in Fig. 6(e). The enlarged views in Fig. 6(b) and (f) reflect the distinct exposure of facets. Under the action of BI_3, BAs crystals present a flat surface. DIC image reveals colorful contrasts on the crystal surface in Fig. 6(c) and monotonous contrasts on the crystal surface in Fig. 6(g). Therefore, BI_3 favors the characteristics of single-crystal growth. I_2 probably produces crystals with defective boundaries, such as twin boundaries, similar to those in the presence of I_2 in the solid-state reactions in Fig. 5(b). SEM images in Fig. 6(d) and (h) show the surface details. As shown in Fig. 6(d), a twin crystal (pointed by yellow arrow) with a shape similar to step-stairs appears in the middle of the isotropic bulk crystal with small crystal facets. The size of the crystal particle is up to 30–50 μm. Meanwhile, crystals with flat hexagonal surfaces grow anisotropically up to a size of ~30 μm. Therefore, the use of BI_3 as a transport agent for CVT can increase the formation probability of single-crystal BAs.

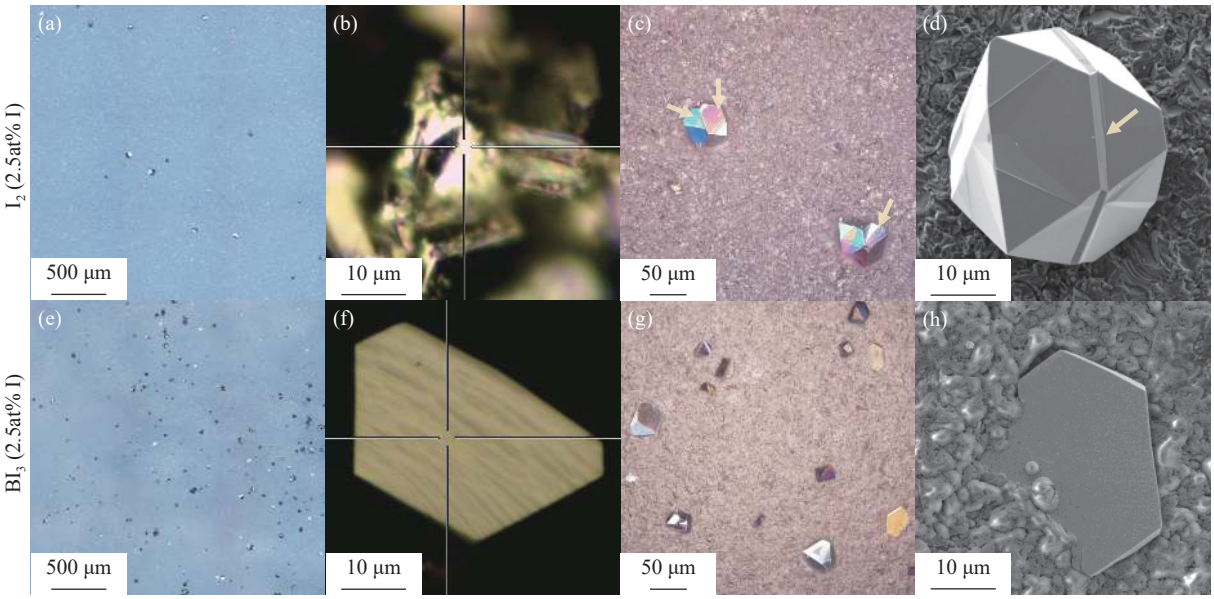

Fig. 6. Morphologies of BAs crystals on the SiO_2 substrate after a growth period of 15 d in CVT: (a–d) regulated by I_2 and (e–f) regulated by BI_3, both at a dose of 2.5at% I; (a, e) optical image with low magnification, (b, f) optical image with high magnification, (c, g) DIC image, and (d, h) SEM image. DIC image in (c) shows defective boundaries (yellow arrows) in colorful contrasts.

In summary, BI_3 accelerates the anisotropic growth of BAs. Even in the solid-state reaction, we can obtain individual BAs crystals and use them as seeds for further growth. BI_3 acts as a coordinator in the synthesis and growth of BAs to maintain the near theoretical stoichiometry ratio and favors defect suppression and anisotropic growth compared with I_2.

4. Conclusions

The role of iodine-containing agents in the reaction between metallic boron and arsenic is discussed in this paper. Agents I_2 and BI_3 accelerate the reaction without the need for extremely high temperatures. The mass fraction of BAs easily increases from ~12% to over 90% at 820°C and 1.5 MPa, a value beyond the promoting effect of only increasing the temperature and pressure. Both agents improve the quality of BAs crystals by reducing FWHM by up to 10%–20%. In particular, I_2 can lead to the agglomeration of BAs crystals with twin defects and the insertion of boron interstitials into the lattice due to the excessive boron supply. BI_3 improves the anisotropy and uniformity of BAs crystals with few defects and maintains the layer spacing of {111} at 0.275 nm and the

stoichiometry ratio (~0.990) approaching 1.0. We confirm the coordinated effect of BI_3 in CVT, and the anisotropic crystals with flat surfaces exhibit monotonous contrast in the DIC image. We conclude that these crystals have single-crystal characteristics. The use of BI_3 favors single-crystal growth, and its coordinated effect can enhance the preparation of BAs crystal seeds and facilitate the advanced application of BAs.

Acknowledgements

This work was financially supported by the National Key R&D Program of China (Nos. 2018YFC1900302 and 2020YFC1909201) and the National Science Fund for Distinguished Young Scholars (No. 51825403).

Conflict of Interest

The authors declare no conflict of interest.

Supplementary Information

The online version contains supplementary material available at https://doi.org/10.1007/s12613-022-2438-z.

References

[1] J.S. Kang, M. Li, H. Wu, H. Nguyen, and Y.J. Hu, Experimental observation of high thermal conductivity in boron arsenide, *Science*, 361(2018), No. 6402, p. 575.

[2] F. Tian and Z.F. Ren, High thermal conductivity in boron arsenide: From prediction to reality, *Angew. Chem. Int. Ed. Engl.*, 58(2019), No. 18, p. 5824.

[3] C. Sealy, Boron arsenide helps devices keep their cool, *Nano Today*, 22(2018), p. 2.

[4] T.L. Feng, L. Lindsay, and X.L. Ruan, Four-phonon scattering significantly reduces intrinsic thermal conductivity of solids, *Phys. Rev. B*, 96(2017), No. 16, art. No. 161201.

[5] N.H. Protik, J. Carrete, N.A. Katcho, N. Mingo, and D. Broido, *Ab initio* study of the effect of vacancies on the thermal conductivity of boron arsenide, *Phys. Rev. B*, 94(2016), No. 4, art. No. 045207.

[6] L. Lindsay, D.A. Broido, and T.L. Reinecke, First-principles determination of ultrahigh thermal conductivity of boron arsenide: A competitor for diamond?, *Phys. Rev. Lett.*, 111(2013), No. 2, art. No. 025901.

[7] Q. Zheng, C.A. Polanco, M.H. Du, L.R. Lindsay, M.F. Chi, J.Q. Yan, and B.C. Sales, Antisite pairs suppress the thermal conductivity of BAs, *Phys. Rev. Lett.*, 121(2018), No. 10, art. No. 105901.

[8] J.A. Perri, S. La Placa, and B. Post, New group III–group V compounds: BP and BAs, *Acta Crystallogr.*, 11(1958), No. 4, art. No. 310.

[9] S.J. Wang, S.F. Swingle, H. Ye, F.R.F. Fan, A.H. Cowley, and A.J. Bard, Synthesis and characterization of a p-type boron arsenide photoelectrode, *J. Am. Chem. Soc.*, 134(2012), No. 27, p. 11056.

[10] J. Kim, D.A. Evans, D.P. Sellan, O.M. Williams, E. Ou, A.H. Cowley, and L. Shi, Thermal and thermoelectric transport measurements of an individual boron arsenide microstructure, *Appl. Phys. Lett.*, 108(2016), No. 20, art. No. 201905.

[11] C.E. Whiteley, Y. Zhang, Y. Gong, S. Bakalova, A. Mayo, J.H. Edgar, and M. Kuball, Semiconducting icosahedral boron arsenide crystal growth for neutron detection, *J. Cryst. Growth*, 318(2011), No. 1, p. 553.

[12] J.W. Pomeroy, M. Kuball, H. Hubel, N.W.A. Van Uden, D.J. Dunstan, R. Nagarajan, and J.H. Edgar, Raman spectroscopy of $B_{12}As_2$ under high pressure, *J. Appl. Phys.*, 96(2004), No. 1, p. 910.

[13] B. Lv, Y.C. Lan, X.Q. Wang, Q. Zhang, Y.J. Hu, A.J. Jacobson, D. Broido, G. Chen, Z.F. Ren, and C.W. Chu, Experimental study of the proposed super-thermal-conductor: BAs, *Appl. Phys. Lett.*, 106(2015), No. 7, art. No. 074105.

[14] F. Tian, B. Song, B. Lv, J.Y. Sun, S.Y. Huyan, Q. Wu, J. Mao, Y.Z. Ni, Z.W. Ding, S. Huberman, T.H. Liu, G. Chen, S. Chen, C.W. Chu, and Z.F. Ren, Seeded growth of boron arsenide single crystals with high thermal conductivity, *Appl. Phys. Lett.*, 112(2018), No. 3, art. No. 031903.

[15] G.A. Gamage, K. Chen, G. Chen, F. Tian, and Z. Ren, Effect of nucleation sites on the growth and quality of single-crystal boron arsenide, *Mater. Today Phys.*, 11(2019), art. No. 100160.

[16] G.A. Gamage, H.R. Sun, H. Ziyaee, F. Tian, and Z.F. Ren, Effect of boron sources on the growth of boron arsenide single crystals by chemical vapor transport, *Appl. Phys. Lett.*, 115(2019), No. 9, art. No. 092103.

[17] H. Sun, K. Chen, G.A. Gamage, H. Ziyaee, F. Wang, Y. Wang, V.G. Hadjiev, F. Tian, G. Chen, and Z. Ren, Boron isotope effect on the thermal conductivity of boron arsenide single crystals, *Mater. Today Phys.*, 11(2019), art. No. 100169.

[18] F. Tian, K. Luo, C.L. Xie, B. Liu, X.W. Liang, L.Y. Wang, G.A. Gamage, H.R. Sun, H. Ziyaee, J.Y. Sun, Z.S. Zhao, B. Xu, G.Y. Gao, X.F. Zhou, and Z.F. Ren, Mechanical properties of boron arsenide single crystal, *Appl. Phys. Lett.*, 114(2019), No. 13, art. No. 131903.

[19] S. Li, Q.Y. Zheng, Y.C. Lv, X.Y. Liu, X.Q. Wang, P.Y. Huang, D.G. Cahill, and B. Lv, High thermal conductivity in cubic boron arsenide crystals, *Science*, 361(2018), No. 6402, p. 579.

[20] J. Xing, E.R. Glaser, B. Song, J.C. Culbertson, J.A. Freitas, R.A. Duncan, K.A. Nelson, G. Chen, and N. Ni, Gas-pressure chemical vapor transport growth of millimeter-sized c-BAs single crystals with moderate thermal conductivity, *Appl. Phys. Lett.*, 112(2018), No. 24, art. No. 241903.

[21] J. Xing, X. Chen, Y.Y. Zhou, J.C. Culbertson, J.A. Freitas, E.R. Glaser, J.S. Zhou, L. Shi, and N. Ni, Multimillimeter-sized cubic boron arsenide grown by chemical vapor transport via a tellurium tetraiodide transport agent, *Appl. Phys. Lett.*, 112(2018), No. 26, art. No. 261901.

[22] T.L. Chu and A.E. Hyslop, Crystal growth and properties of boron monoarsenide, *J. Appl. Phys.*, 43(1972), No. 2, p. 276.

[23] J.L. Lyons, J.B. Varley, E.R. Glaser, J.A. Freitas, J.C. Culbertson, F. Tian, G.A. Gamage, H.R. Sun, H. Ziyaee, and Z.F. Ren, Impurity-derived p-type conductivity in cubic boron arsenide, *Appl. Phys. Lett.*, 113(2018), No. 25, art. No. 251902.

[24] H. Detz, D. MacFarland, T. Zederbauer, S. Lancaster, A.M. Andrews, W. Schrenk, and G. Strasser, Growth rate dependence of boron incorporation into $B_xGa_{1-x}As$ layers, *J. Cryst. Growth*, 477(2017), p. 77.

[25] H. Dumont, D. Rutzinger, C. Vincent, J. Dazord, Y. Monteil, F. Alexandre, and J.L. Gentner, Surface segregation of boron in $B_xGa_{1-x}As$/GaAs epilayers studied by X-ray photoelectron spectroscopy and atomic force microscopy, *Appl. Phys. Lett.*, 82(2003), No. 12, p. 1830.

[26] F. Tian, B. Song, X. Chen, N.K. Ravichandran, Y.C. Lv, K. Chen, S. Sullivan, J. Kim, Y.Y. Zhou, T.H. Liu, M. Goni, Z.W. Ding, J.Y. Sun, G.A.G. Udalamatta Gamage, H.R. Sun, H. Ziyaee, S.Y. Huyan, L.Z. Deng, J.S. Zhou, A.J. Schmidt, S. Chen, C.W. Chu, P.Y. Huang, D. Broido, L. Shi, G. Chen, and Z.F. Ren, Unusual high thermal conductivity in boron arsenide bulk crystals, *Science*, 361(2018), No. 6402, p. 582.

[27] W. Klement, A. Jayaraman, and G.C. Kennedy, Phase diagrams of arsenic, antimony, and bismuth at pressures up to 70 kbars, *Phys. Rev.*, 131(1963), No. 2, p. 632.
[28] A.F. Armington, Vapor transport of boron, boron phosphide and boron arsenide, *J. Cryst. Growth*, 1(1967), No. 1, p. 47.
[29] J. Bouix and R. Hillel, Chemical transport of BAs and BP, *J. Less-Common Met.*, 47(1976), p. 67.
[30] V.G. Hadjiev, M.N. Iliev, B. Lv, Z.F. Ren, and C.W. Chu, Anomalous vibrational properties of cubic boron arsenide, *Phys. Rev. B*, 89(2014), No. 2, art. No. 024308.
[31] S.M. Londoño-Restrepo, L.F. Zubieta-Otero, R. Jeronimo-Cruz, M.A. Mondragon, and M.E. Rodriguez-García, Effect of the crystal size on the infrared and Raman spectra of bio hydroxyapatite of human, bovine, and porcine bones, *J. Raman Spectrosc.*, 50(2019), No. 8, p. 1120.
[32] J.J. Wang, D. Chen, Y. Xu, Q.X. Liu, and L.Y. Zhang, Influence of the crystal texture on Raman spectroscopy of the AlN films prepared by pulse laser deposition, *J. Spectrosc.*, 2013(2013), art. No. 103602.
[33] X.H. Meng, A. Singh, R. Juneja, Y.Y. Zhang, F. Tian, Z.F. Ren, A.K. Singh, L. Shi, J.F. Lin, and Y.G. Wang, Pressure-dependent behavior of defect-modulated band structure in boron arsenide, *Adv. Mater.*, 32(2020), No. 45, art. No. e2001942.
[34] M. Endo, H. Uchiyama, Y. Ohno, and J. Hirotani, Temperature dependence of Raman shift in defective single-walled carbon nanotubes, *Appl. Phys. Express*, 15(2022), No. 2, art. No. 025001.